JOURNAL OF AIRCRAFT
Vol. 31, No. 1, Jan.–Feb. 1994

Investigation of Three-Dimensional Separation at Wing/Body Junctions in Supersonic Flows

B. Lakshmanan* and S. N. Tiwari†
Old Dominion University, Norfolk, Virginia 23529

The problem of three-dimensional separation at a wing/body junction has been investigated numerically using a three-dimensional Navier-Stokes code which employs the MacCormack's time split, finite volume technique. An algebraic grid generation technique is used for generating the grid at a wing/body junction. Specific computational results on velocity and pressure distribution in the separated flow region are compared with the experimental results. A parametric study of flow parameters, such as Mach and Reynolds numbers, have been carried out to understand their effect in interaction flowfield. The parametric study indicates dependency of the number of vortices at the junction on Mach number and Reynolds number.

Nomenclature

a	=	speed of sound
CFL	=	Courants-Friedrichs-Lewy number
D	=	diameter of the fin
E	=	total energy per unit mass
e_i	=	specific internal energy, $T/\gamma(\gamma - 1)$
H	=	height of the fin
i	=	grid index in ξ direction
j	=	grid index in η direction
k	=	grid index in ζ direction
$L\xi$, $L\eta$, $L\zeta$	=	finite difference operators in ξ, η, and ζ direction
M	=	Mach number
p	=	static pressure
Pr_l	=	laminar Prandtl number
Pr_t	=	turbulent Prandtl number
q	=	vector of conserved variables
Re_1	=	unit Reynolds number
T	=	static temperature
t	=	time
u	=	velocity component in x direction
v	=	velocity component in y direction
w	=	velocity component in z direction
x, y, z	=	Cartesian coordinates
γ	=	ratio of specific heat, c_p/c_v
Δt	=	time steps used for $L\xi$, $L\eta$, and $L\zeta$ operators
δ	=	boundary-layer thickness
λ	=	second coefficient of viscosity $-\frac{2}{3}\mu$
μ	=	dynamic molecular viscosity
ξ, η, ζ	=	body-oriented coordinates
ρ	=	density
σ	=	safety factor in the stability criteria equation

Subscripts

e	=	evaluated at the boundary-layer edge corresponding to $u/u_e = 0.995$
∞	=	evaluated in freestream conditions

Received Feb. 24, 1992; revision received Aug. 3, 1992; accepted for publication Oct. 30, 1992.

*Research Associate, Department of Mechanical Engineering and Mechanics. Member AIAA.

†Eminent Professor, Department of Mechanical Engineering and Mechanics. Associate Fellow AIAA.

Introduction

MANEUVERING flight vehicles operating from subsonic to supersonic speeds encounter three-dimensional separation at several intersecting surfaces such as wing-fuselage and wing-pylong junctions, and air breathing engine inlets. The flow originating at the intersecting surfaces depicts complex flow patterns which may significantly affect the performance of the aircraft. The major effects are increased pressure and heat transfer level in the vicinity of the intersections, and loss of control effectiveness due to flow separation. Thus, the prediction and control of complex three-dimensional separated flows is of vital importance to the aircraft designer. A variety of simplified geometrical configurations have been studied to understand the physical aspects of three-dimensional separated flows. Some of these include 1) sharp fin-mounted on a flat plate, 2) blunt fin-mounted on a flat plate, 3) swept compression corner, and 4) semicone affixed to a flat plate.

In this article, we consider the high-speed flow past a blunt fin/flat plate junction (Fig. 1) which is a typical example of junction flow. This flowfield is characterized by the presence of shock waves in the flowfield, in addition to the vortical

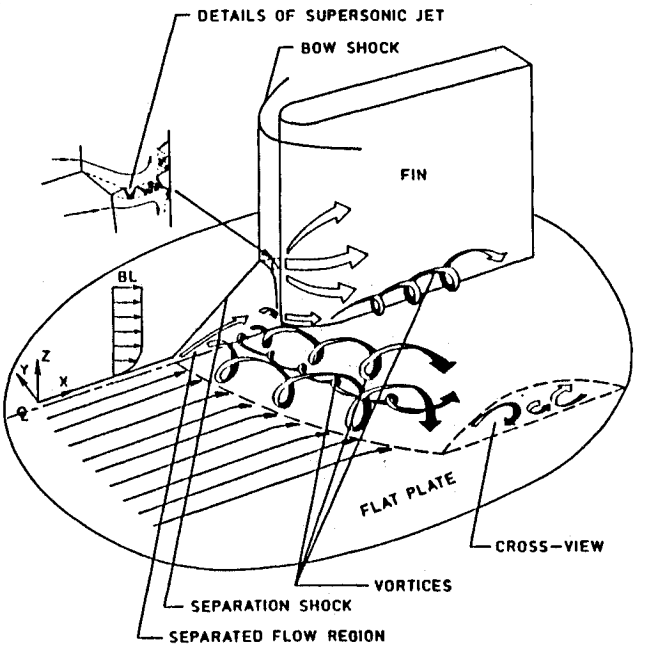

Fig. 1 Simplified flow structure at the blunt fin/flat plate junction.

structures observed at low speed. The detached bow shock formed ahead of the fin induces a strong adverse pressure gradient to the flat plate boundary layer. This results in a separated flow region composed of horseshoe vortices downstream of the separation point, and a lambda shock in the plane of symmetry. Immediately downstream of the primary separation point, there appears to be one or more vortices depending on the geometric and flow parameters. A strong corner vortex originates at the fin root and remains downstream as a trailing vortex. In addition, the separation shock (incoming shock) emanating from the separated flow region, impinges on the fin bow shock resulting in a shock-shock interaction. Depending on the severity of the incoming shock, the shock-shock interaction could lead to the formation of supersonic jet. The flow in the supersonic jet passes through several oblique shocks (see the enlarged view of supersonic jet in Fig. 1) and is compressed nearly isentropically, leading to extremely large pressure and high heat transfer locally on the fin leading edge and adjoining regions of the fin root. However, in the present study, the incoming shock generated due to flow separation was weak, and therefore, the supersonic jet was not observed.

Three-dimensional shock wave and boundary-layer interacting flows, induced by circular cylinders or hemispherically blunted fins in supersonic boundary layers, have been the subject of extensive experimental and analytical research over the past few years. A juncture flow problem was investigated experimentally by Sedney[1] using a flow visualization technique. The main objective of the experiment was to correlate the separation distance as a function of Mach number, Reynolds number, and obstacle dimensions. It was found that the primary separation distance of the flow is dependent both on the Mach number and obstacle height, but only weakly dependent on the Reynolds number. However, the structure of the flow upstream of the protuberance was found to change with relatively small changes in the Reynolds number. Experiments have been carried out by previous investigators on a class of related problems to study the effect of diameter of the fin,[2-11] height of the protuberance,[2,4,7] incoming boundary-layer thickness,[2,6,8,9] and Reynolds number[2,4,9,12,13] on the interaction. Attempts have been made to correlate the experimental data, but confusion over the conditions necessary for the model to be considered semi-infinite have caused difficulty, particularly with respect to the vertical scale of the flowfield. However, most of the experiments revealed clearly that the dominant parameters controlling the centerline flowfield are the diameter and sweep angle of the fin. Dolling et al.[10,11] examined the spanwise extent of the disturbed flowfield. The first objective of the experiment was to investigate the spanwise development of the disturbed flowfield and to determine its dependence on the model geometry and incoming flow conditions. The second objective of the experiment was to determine the vertical extent of the interaction on the fin. The results show that, on the test surface near the fin and on the fin itself, the leading-edge diameter plays a dominant role in determining the interaction scale and characteristics. Özcan and Holt[14] recently investigated the high-speed laminar flow characteristics of a circular cylinder on a flat plate using the oil flow visualization technique. For the flow conditions considered, the extent of separation was found to be independent of the cylinder height-to-diameter ratio greater than approximately four. Large streamwise and spanwise pressure gradients were observed within an approximate distance of 2-cylinder diameter from the axis. The velocity measurements indicated a highly unsteady flow structure. Hung and Kordulla[15] and Hung and Bunning[16] studied numerically the blunt fin induced shockwave/turbulent boundary-layer interaction using the compressible Navier-Stokes equations. It was noted that varying the incoming boundary-layer thickness by an order of magnitude, showed that the size of the horseshoe vortex and the spatial extent of the interaction are dominated by inviscid effects, and are only weakly dependent on the Reynolds number. Hung[17] also noted that by changing the blunt fin to flat-faced fin, the extent of separation increased dramatically, and the main horseshoe vortex bifurcated into two vortices rotating in the same direction.

Owing to the complexity of the problem, most of the experimental study have concentrated on obtaining the flow characteristics in the plane of symmetry and selected spanwise locations. With availability of vector processors like Cray II and Cyber 205, solutions of three-dimensional Navier-Stokes equations for realistic configurations are now possible. The primary objective of this study is to understand laminar three-dimensional separation in a junction flow, and examine the essential questions of concern such as grid resolution in the flowfield. Another motive of the study is to investigate the effect of flow parameters on the number of vortices produced at the junction.

Physical Model and Theoretical Formulation

The physical model and coordinate system for the flow past a blunt fin/flat plate junction[9] are shown in Fig. 1. As mentioned in the introduction, a high-speed flow past such configurations results in a complex flow structure with viscous-inviscid and shock-shock interactions. The essential features of the flowfield are shown in the figure in a simplified form.

The theoretical formulation of the problem starts with the nondimensional form of the compressible three-dimensional Navier-Stokes equations cast in the generalized body-oriented coordinate system. Specifically, the integral form of the Navier-Stokes equations without external body forces and source terms is used, and this is expressed as[16]

$$\frac{\partial}{\partial t}\int_v \boldsymbol{q}\,\mathrm{d}v + \int_s (\boldsymbol{q}\underline{u} + \underline{b})\cdot\underline{n}\,\mathrm{d}s = 0 \tag{1}$$

where

$$\boldsymbol{q} = (\rho, \rho u, \rho v, \rho w, \rho E)^T$$

$$E = e_i + \tfrac{1}{2}(u^2 + v^2 + w^2)$$

$$\underline{b} = (\underline{b}_\rho, \underline{b}_m, \underline{b}_e)^T, \qquad \underline{b}_\rho = 0$$

$$\underline{b}_m = p\underline{\underline{I}} + M_\infty Re_D^{-1}\underline{\underline{\tau}}$$

$$\underline{\underline{\tau}} = -\lambda\,\mathrm{div}\,\underline{u}\,\underline{\underline{I}} - \mu[(\mathrm{grad}\,\underline{u}) + (\mathrm{grad}\,\underline{u})^T]$$

$$\underline{b}_e = -\gamma M_\infty (Re_D Pr)^{-1}\mu\,\mathrm{grad}\,e_i + p\underline{u} + M_\infty Re_D^{-1}\underline{\underline{\tau}}\cdot\underline{u}$$

The nondimensionalization of the governing equations is carried out by normalizing the Cartesian velocity components (u, v, w) by a_∞, ρ by ρ_∞, e_i, E by a_∞^2, and p by $\rho_\infty a_\infty^2$. The viscosity coefficients λ and μ are normalized by the molecular viscosity μ_∞. The governing equations are further supplemented by the following equations of state:

$$p = (1/\gamma)\rho T; \qquad e_i = T/\gamma(\gamma - 1); \qquad a^2 = T \tag{2}$$

where T is normalized by the freestream static temperature.

The above system of equations is assumed to be valid for turbulent flows if the molecular transport coefficients are replaced by

$$\mu = \mu_l + \mu_t \tag{3a}$$

$$(\mu/Pr) = (\mu_l/Pr_l) + (\mu_t/Pr_t) \tag{3b}$$

where μ_t represents the turbulent eddy viscosity. The molecular dynamic viscosity is evaluated using the Sutherland's law of viscosity. The code employs Baldwin and Lomax turbulence model,[18] the details of which can be found in Ref. 16.

Thin-Layer Approximation

For high-Reynolds number flows, the effects of viscosity are confined to a thin layer near the wall boundary. In this region, the viscous terms in the normal direction dominate the flow and the viscous effects along the body direction are usually small and negligible. The development of thin-layer approximation by Baldwin and Lomax[18] is based on this concept, with the retention of the unsteady and all the inviscid terms of the Navier-Stokes equations. The extension of thin-layer approximation to two directions was demonstrated in a previous study of supersonic flow over an axial corner.[19] Here, the concept is extended to the case of thin layers in all three directions for a general coordinate system. All the viscous terms associated with the cross derivatives are neglected compared to normal second derivative terms. The neglected cross derivatives near the wall can be of the same order of magnitude as the normal derivatives, but the flow there contains comparatively very low momentum fluid, and therefore, such an approximation will not significantly influence the flow at the junction. The use of thin-layer approximation greatly simplifies evaluation of the viscous terms, and allows easy vectorization of the algorithm.

Boundary and Initial Conditions

The fin is assumed to be semi-infinite in height and length. Consequently, zeroth-order extrapolations can be applied in these directions. The fin is assumed to be at zero angle of attack, and a symmetry boundary condition is imposed at the plane of symmetry. The wall is assumed impermeable, and no-slip and no penetration boundary conditions are applied. The wall conditions are also assumed to be adiabatic and the pressure has a zero gradient normal to the wall.

The outer boundary $J = J_{max}$ is set far away to avoid any influence on the interaction region. Since the flow is boundary-layer like at these locations, theoretically one can specify a boundary-layer profile on the flat plate at each axial location along the outer boundary. These profiles can be easily generated from their corresponding points of a flow over an isolated flat plate using a boundary-layer code. In the present study, the region of interest is assumed small compared to the length of the flat plate generating the incoming boundary-layer profile. Hence, the variation of the boundary-layer profile at the outer boundary is assumed small and is neglected. Therefore, one predetermined boundary-layer profile is prescribed for all x locations along the outer boundary.

The initial conditions required to initiate the computation is obtained by simply propagating the specified boundary-layer profiles at $J = J_{max}$ everywhere in the computational domain. To correct the erroneous occurrence of negative density in the flowfield, and thereby allowing a large CFL number to be used during the startup phase, the blunt body starting condition as suggested in Ref. 15 is used.

Method of Solution

Grid Generation

As shown in Fig. 2, an algebraic grid generaton technique is used to generate the mesh at the blunt fin/flat plate junction. The grid lines are clustered near the plate and fin surfaces using a geometric stretching formula to provide adequate resolution of the viscous effects. The three-dimensional grid employed in the flow computation is generated by rotating the grid in the plane of symmetry about the fin leading edge. Since the flow is assumed to be symmetric, only one-half of the flow is computed.

Computational Procedures

The computer program used in this study is coded for a three-dimensional generalized body-fitted coordinate system. As such, varous geometries can be handled by the code. The code employs the MacCormack's explicit predictor-corrector method,[20] using the time-split finite volume technique.

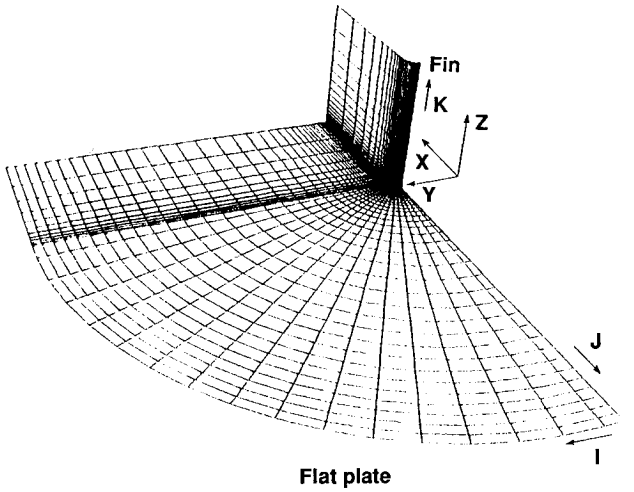

Fig. 2 Mesh distribution on the blunt fin and flat plate.

The time-splitting reduces the complex three-dimensional operators into a sequence of three one-dimensional operators. Thus, split operator contains the spatial flux derivatives and artificial dissipation terms in only one direction. The finite difference formulation in terms of the split operators can be expressed as

$$\hat{q}^{n+2} = L\eta(\Delta t)L\zeta(\Delta t)L\xi(2\Delta t)L\zeta(\Delta t)L\eta(\Delta t)\hat{q}^{n} \qquad (4)$$

Each split operator consists of a predictor and corrector steps. During a specific numerical sweep the inviscid fluxes are forward-differenced in the prediction sequence and backward-differenced in the correction step. The viscous fluxes are always centrally-differenced. The composite numerical method is second-order accurate in both time and space, and is conditionally stable requiring no scalar or block tridiagonal inversions. Artificial smoothing terms are explicitly added to the fluxes to stabilize the numerical scheme when computing flows with strong shocks. Since an explicit scheme is utilized in the present study, the time step used for integrating the governing equations is restricted by the stability criteria. Because of the complex nature of the compressible Navier-Stokes equations, it is not possible to obtain a closed-form stability expression for the MacCormack scheme applied to these equations. However, the following empirical formula can normally be employed:

$$\Delta t \leq \sigma(\Delta t)_{CFL} \qquad (5)$$

In Eq. (5), σ is the safety factor ($\approx$0.9) for viscous problems and $(\Delta t)_{CFL}$ is the inviscid CFL condition given by

$$(\Delta t)_{CFL} \leq \left[\frac{|u|}{\Delta x} + \frac{|v|}{\Delta y} + \frac{|w|}{\Delta z} + a\sqrt{\frac{1}{(\Delta x)^2} + \frac{1}{(\Delta y)^2} + \frac{1}{(\Delta z)^2}}\right]^{-1} \qquad (6)$$

where a is the local speed of sound.

Physical Conditions of Investigation

A simple blunt fin/flat plate geometry is chosen for computational study because extensive measurements on velocity and pressure distribution in the separated flow region are easily available in the literature. In a typical three-dimensional flow, past a fin/flat plate junction, the various parameters controlling the interaction are D, H, δ, M_∞, and Re_l. Since three-dimensional computations are expensive, only limited parametric studies were carried out for selected values of

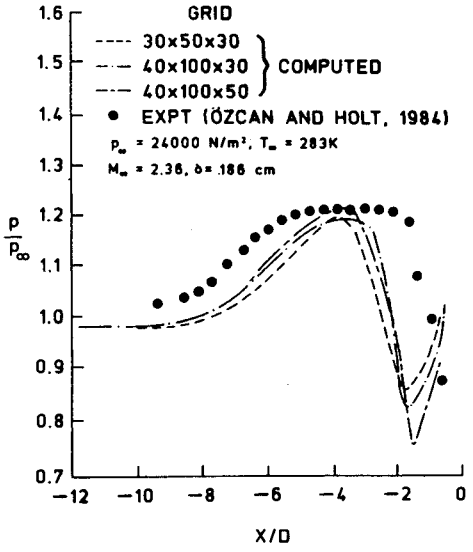

Fig. 3 Comparison of pressure distribution along the line of symmetry.

Mach and Reynolds numbers. The range of values in each set of parameters is carefully selected to portray its dramatic influence in controlling the intersection flowfields.

The following specific conditions were selected to validate the computed results with the experimental measurements[14]:

$$M_\infty = 2.36, \quad P_{0\infty} = 24{,}000 \text{ N/m}^2, \quad T_{0\infty} = 294 \text{ K}$$

$$\delta = 0.186 \text{ cm}, \quad D = 0.635 \text{ cm}, \quad H = 5 \text{ cm}$$

A blunt fin/flat plate junction was selected to validate the code with the experimental measurement on velocity distribution in the separated flow region. The experimental measurements were obtained by oil flow visualization, schlieren observations, and laser anemometry, and the results are available in Ref. 14.

Before carrying out the parametric study of the flow variables, the computed results are validated with experimental measurements using three different grid resolutions. To investigate the effect of grid refinement, the conditions given above were used and results were obtained for the following three grids:

$$30 \times 50 \times 30, \quad 40 \times 100 \times 30, \quad 40 \times 100 \times 50$$

The effect of grid refinement on the wall pressure distribution along the line of symmetry is shown in Fig. 3. It is noted that computations using different grids yield nearly identical results in the region $12 < (-X/D) < 2$, and slightly underpredict the extent of separation. In the region $2 < (-X/D) < 0$, somewhat different results are obtained using different grids.

The effects of grid refinement on computed axial velocity profiles are shown in Fig. 4 for various X/D locations. It is seen, from the results presented in Figs. 4a and 4b, that grid independent results are obtained at different X/D locations by using the $40 \times 100 \times 30$ mesh. Even though the flow is laminar at the separation point, agreement between the experiment and computations at X/D locations shown in Figs. 4a and 4b is only satisfactory due to the transitional nature of the flow in the separated region. However, the agreement between the computed results and the experimental data at locations $X/D = -2.4$ and -1.6 (Fig. 4c) is not very good in spite of the highly resolved flow; this, possibly, suggests that the flow is turbulent at these locations.

The effects of grid refinement on computed normal velocity profiles are shown in Fig. 5 for various X/D locations. At

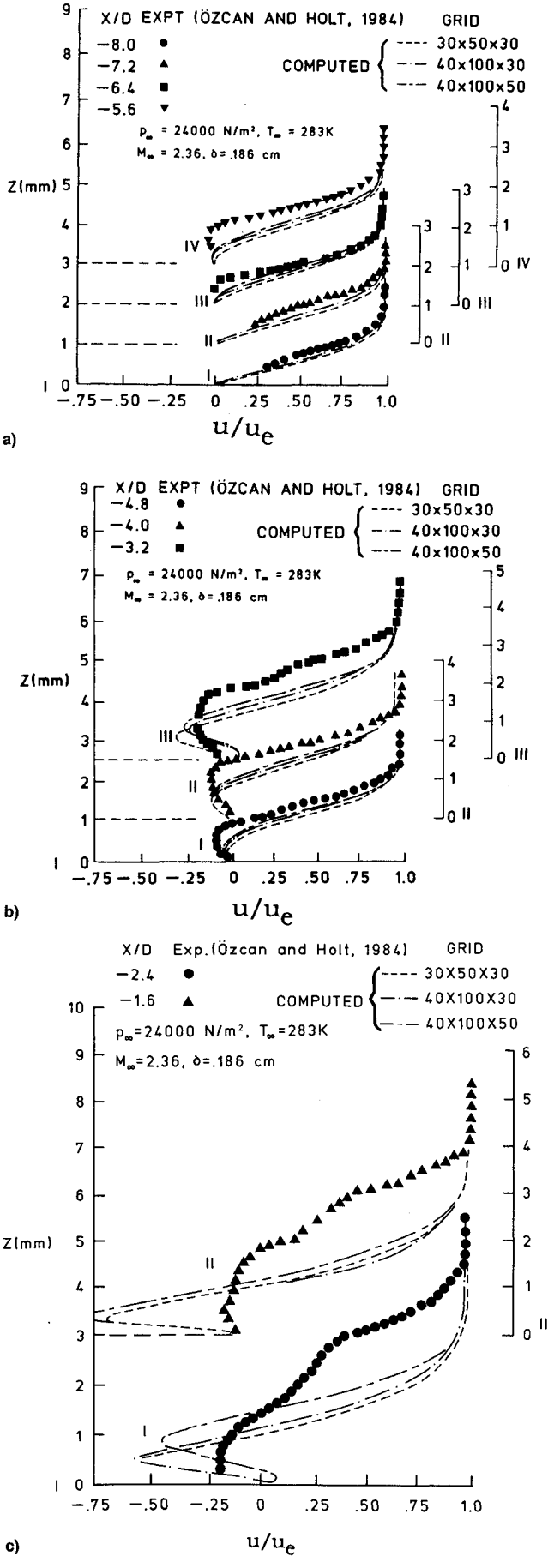

Fig. 4 Comparison of streamwise velocity profile along a) $X/D = -8$, -7.2, -6.4, and -5.6; b) $X/D = -4.8$, -4, and -3.2; and c) $X/D = -2.4$ and -1.6.

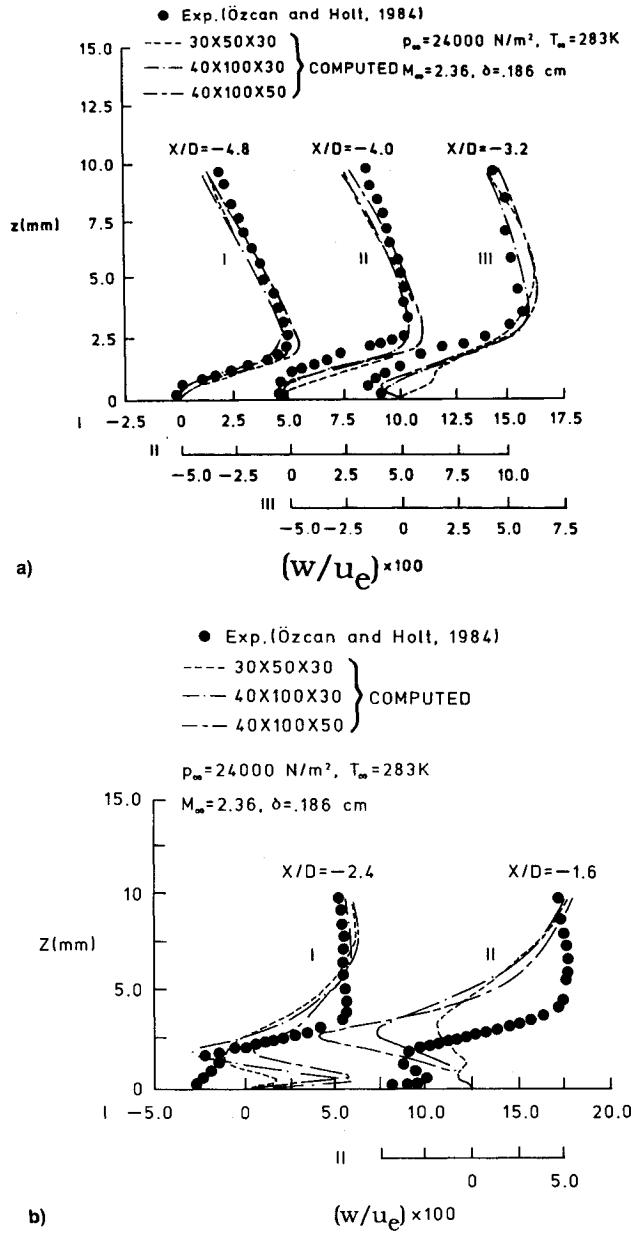

Fig. 5 Comparison of normal velocity profile along a) $X/D = -4.8$, -4, and -3.2 and b) $X/D = -2.4$ and -1.6.

locations $X/D = -4$ and -3.2, the velocity profiles obtained by using the 30 × 50 × 30 mesh show some discrepancy with the experiment for z locations less than 2.5 mm (Fig. 5a). However, computations using the finer grids (40 × 100 × 30) and (40 × 100 × 50) are able to improve the prediction at these locations. Moreover, the variation in the computed solution using the two fine grids, 40 × 100 × 30 and 40 × 100 × 50, was found to be minimum. The computed normal velocity profiles at locations $X/D = -2.4$ and -1.6 show considerable deviation from the experimental data (Fig. 5b). The reason for this is given in the explanation of results presented in Fig. 4c.

Although the computed results displayed some sensitivity to grid refinement, the overall topology of the flow (number of vortices) was unchanged. Based on these observations, and for computational economy, it was decided to carry out the parametric study using the 40 × 100 × 30 grid, referred hereafter as the "baseline mesh."

The effect of Mach number is investigated by changing the freestream stagnation temperature corresponding to each Mach number, while keeping the other conditions constant as given in the experiment. The results were obtained for the following cases:

$$M_\infty = 1.2, \quad T_{0\infty} = 286 \text{ K}$$
$$M_\infty = 2.36, \quad T_{0\infty} = 294 \text{ K}$$
$$M_\infty = 3.5, \quad T_{0\infty} = 307 \text{ K}$$

The effect of Reynolds number is investigated by changing the tunnel stagnation pressure while keeping the other freestream conditions constant as given in the experiment. The results were obtained for the following cases:

$$P_{0\infty} = 12{,}000 \text{ N/m}^2, \quad Re_l = 1.25 \times 10^6/\text{m}$$
$$P_{0\infty} = 24{,}000 \text{ N/m}^2, \quad Re_l = 2.5 \times 10^6/\text{m}$$
$$P_{0\infty} = 48{,}000 \text{ N/m}^2, \quad Re_l = 5 \times 10^6/\text{m}$$

Results and Discussion

The results obtained for the physical conditions described in the last section are presented here. For the physical conditions where experimental results were available, numerical results were obtained to validate the computer code developed in this study. For the sake of brevity, only key results are presented here. Extensive results were obtained for other physical conditions to study the behavior of three-dimensional separation in high-speed junction flows. The effect of different parameters in controlling the intersection flowfield were also investigated and the details are given in Ref. 21.

Comparison of Computations with Experimental Data

Numerical results obtained by using the baseline mesh (40 × 100 × 30) are compared with experimental data. The pressure distribution along the axis of symmetry is shown in Fig. 3. It is apparent that in the experiment the pressure begins to rise at about 10-diam upstream of the fin leading edge. The separation occurs, in the experiment, further downstream ($X/D = -6.8$) between the regions of initial pressure rise and pressure plateau. The pressure reaches a valley downstream of the plateau region and then increases across the detached bow shock. For the sake of clarity, the vertical distance is stretched and the pressure jump across the bow shock is omitted in Fig. 3. Typically the pressure jumps by a factor

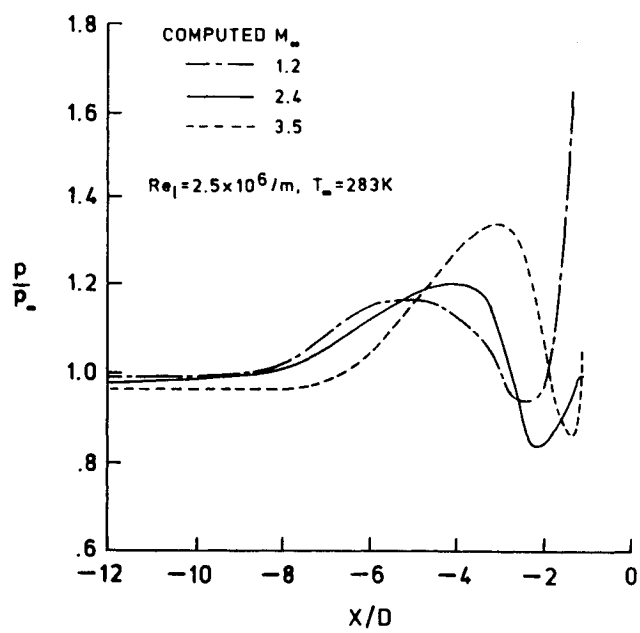

Fig. 6 Pressure distribution along the line of symmetry for various Mach numbers.

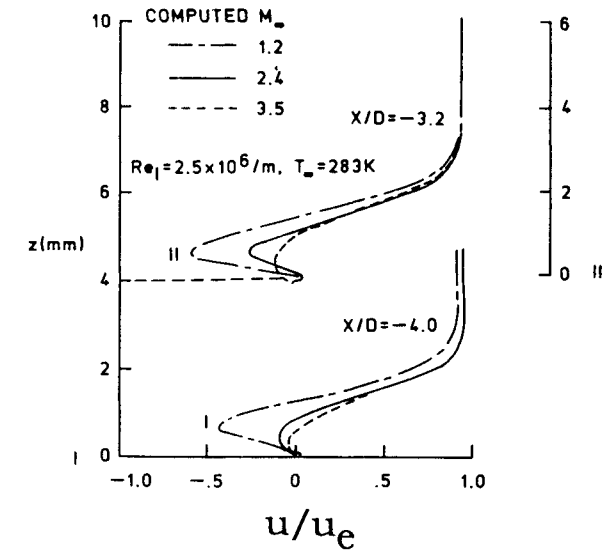

Fig. 7 Streamwise velocity profiles for various Mach numbers along $X/D = -4$ and -3.2.

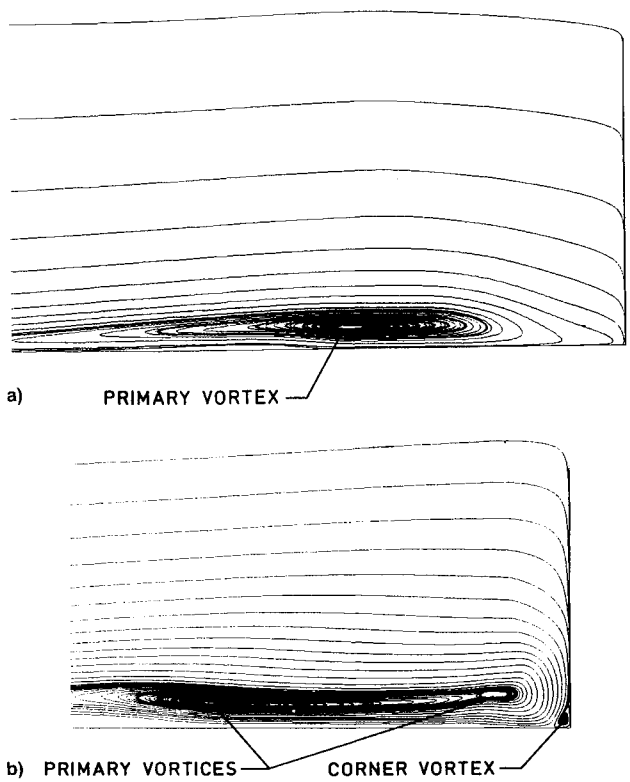

Fig. 8 Particle paths in the plane of symmetry for various Mach numbers a) $M_\infty = 1.2$ and b) $M_\infty = 2.36$ and $Re_l = 2.5 \times 10^6$ m^{-1}.

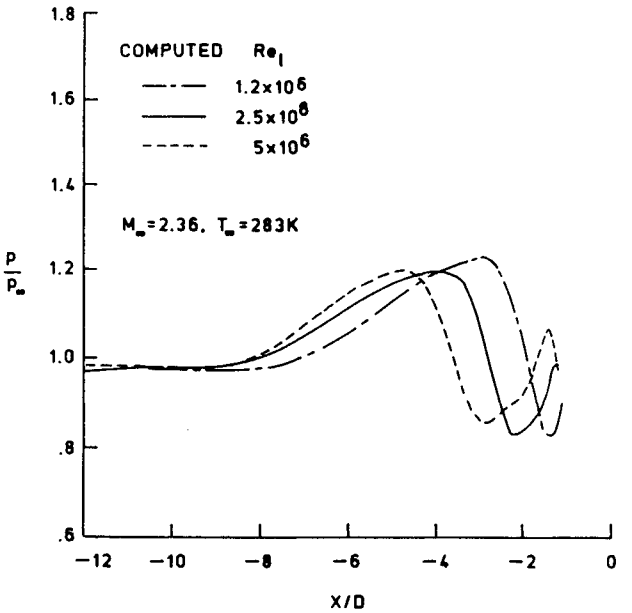

Fig. 9 Pressure distribution along the line of symmetry for various unit Reynolds number.

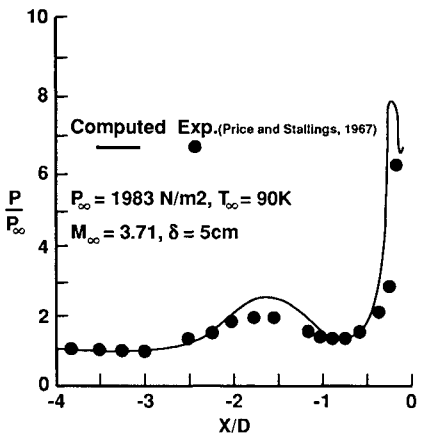

Fig. 10 Pressure distribution along the line of symmetry for a turbulent flow past a blunt fin/flat plate junction.

of 9 across the bow shock. The computed results, using the baseline mesh, slightly underpredict the extent of separation. However, the agreement between the computed and experimental results is not very good in the downstream region. Computations using the refined mesh (discussed under grid resolution) did not show significant improvement to the results in this region. Furthermore, the computed results fail to predict the length of the pressure plateau region observed in the experiment. The discrepancy between the computed results and the experimental values is due to the flow going through transition to turbulence in this region.

The computed and the experimentally measured streamwise velocity profiles along the line of symmetry are shown in Fig. 4. The streamwise velocity component is nondimensionalized with reference to the velocity u_e at the edge of the boundary layer. The dashed lines along the vertical axis show the displaced origin to avoid overcrowding of the figures. In general, the agreement between the computation and the experiment is satisfactory, except the location and height of the separated flow region are slightly underpredicted by the numerical code. Specifically, the computations predict the separation location around $X/D = -5.6$. The streamwise velocity profiles along $X/D = -8$ and -7.2 (Fig. 4a) indicate preseparation behavior. The velocity profile at $X/D = -6.4$ indicates that the separation occurs in the close vicinity of $X/D = -6.4$. In the experiment, the separation occurs around $X/D = -6.8$. However, it was difficult to make repeatable measurements at that location due to the inherent unsteadiness of the flow. Also, due to the small scale of the reversed flow region at $X/D = -6.4$, it was found difficult to detect the reversed flow region in the vicinity of the primary separation line. The velocity profile at $X/D = -5.6$ clearly shows the reversed flow region. The velocity profiles at $X/D = -4.8$, -4, and -3.2 are shown in Fig. 4b. These results show that the magnitude and height of the reversed flow region increases with increasing X/D. The velocity profile at axial locations corresponding to $X/D = -2.4$ and -1.6 are shown in Fig. 4c. The experimental results show that the magnitude of the maximum reverse velocity is approximately constant.

In contrast, the computed results show that the magnitude of the maximum reverse velocity is increasing with decreasing $-X/D$. All the profiles shown at axial locations (Figs. 4b and 4c) display postseparation behavior. The measured streamwise velocity profiles at $X/D = -3.2$, -2.4, and -1.6 display a significant kink between the boundary-layer edge and the edge of the reversed flow region. However, the computed velocity profiles do not display such behavior.

The normal velocity profiles at various axial locations are shown in Fig. 5. For all the profiles, the maximum normal velocity occurs around the boundary-layer edge (corresponding to $u/u_e \simeq 0.99$) and then decreases with increasing z in the freestream. Maximum reverse velocities (in the direction towards the plate) and height of the reversed flow region increases with decreasing $-X/D$.

Effect of Mach Number

The effect of Mach number on the pressure distribution in the plane of symmetry is shown in Fig. 6 using a 40 × 100 × 30 mesh. The effect of increasing the Mach number is to decrease the extent of separation ahead of the fin. Young et al.[22] observed a smaller separation region at $M_\infty = 5$ as compared to $M_\infty = 3$. Also, the magnitude of the pressure, following separation, increases with an increase in the Mach number.

The streamwise velocity profiles for various Mach numbers are shown in Fig. 7 at selected X/D stations (corresponding to locations underneath the core of the primary vortex). The effect of increasing the Mach number is to decrease the maximum reverse velocity near the flat plate. Furthermore, the height of the reversed flow region above the flat plate decreases with an increase in the freestream Mach number. The simulated particle paths (in the plane of symmetry) at various Mach numbers are shown in Fig. 8. Only the particle paths corresponding to $M_\infty = 1.2$ and 2.36 are shown. The vortical structure of the flow at $M_\infty = 3.5$ displayed no abrupt change from $M_\infty = 2.36$. At $M_\infty = 1.2$ (Fig. 8a), only a single vortex rotating in the clockwise direction can be seen, as opposed to multivortex patterns observed at higher Mach numbers (Fig. 8b). Similar trend in flow patterns was observed by Baker[23] in low-speed laminar flow where the number of vortices at the junction increased with increase in freestream velocity. An interesting feature of Fig. 8b is the concave nature of the streamlines connecting the two primary vortices.

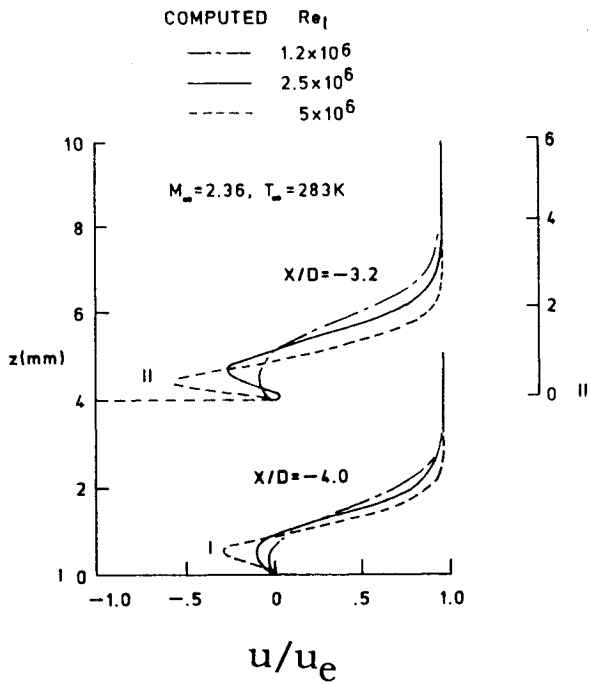

Fig. 11 Streamwise velocity profiles for various unit Reynolds number along $X/D = -4$ and -3.2.

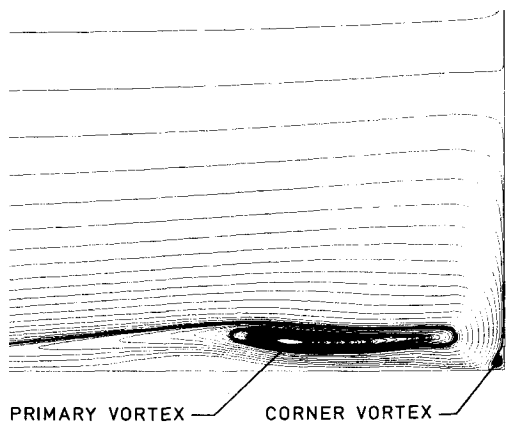

Fig. 12 Particle paths in the plane of symmetry for unit Reynolds number $Re_l = 1.25 \times 10^6$ m^{-1}.

Effect of Reynolds Number

The effect of unit Reynolds number on the pressure distribution along the line of symmetry is shown in Fig. 9. The effect of increasing the Reynolds number is to move the location of the pressure rise, following separation, outboard from the fin leading edge. In the experiment carried out by Özcan and Holt,[14] in laminar supersonic junction flows, it was observed that separation increases with an increase in the Reynolds number. It was also noted that the separation distance is independent of H/D as long as it is greater than 3.5. To understand the effect of fully turbulent flow on the extent of separation numerical results were obtained by using the Baldwin and Lomax turbulence model,[18] and compared with the experimental data of Price and Stallings.[4] The results are shown in Fig. 10. It is clear that when the flow is fully turbulent, the extent of separation decreases dramatically (to 2-diam ahead of the fin leading edge), as opposed to larger separation observed in laminar flows. Also, the magnitude of pressure, following separation, increases to a value of about 2.8 as compared to a value of 1.4 observed in laminar flows.

The streamwise velocity profile at $X/D = -4$ and -3.2 (corresponding to locations underneath the core of the primary vortex) shown in Fig. 11, demonstrate that the maximum reverse velocity near the plate increases with an increase in the Reynolds number. The flow structure at Reynolds number equal to 1.25×10^6 m^{-1} shows the presence of two vortices corresponding to primary and corner vortices (Fig. 12). As the Reynolds number is increased to 2.5×10^6 m^{-1}, the primary vortex bifurcates into two vortices rotating in the same direction (see also Fig. 8b). Similar topological phenomena were observed in Ref. 24 where the number of vortices increased with an increase in Reynolds number.

Conclusions

The supersonic laminar flow past a wing/body junction is simulated numerically using a three-dimensional Navier-Stokes code. Results have been obtained for a simplified geometry such as blunt fin/flat plate junction. In general, the agreement between the computed results and experimental values for velocity and pressure distribution in the separated flow region is satisfactory. However, the computed results demonstrate that better agreement with experimental results can be obtained by refining the mesh. The parametric study of Mach and Reynolds number variation reveals the dependency of the number of vortices (at the junction) with flow parameters. Moreover, with an increase in the freestream Mach and Reynolds numbers, the primary horseshoe vortex bifurcated into two vortices rotating in the same direction. The saddle point of attachment observed in Ref. 24 could not be confirmed for

the Mach and Reynolds numbers considered in the present study. Further research in transition and turbulence modeling is necessary to understand the dynamic nature of the flowfield.

Acknowledgments

This work was supported by the NASA Langley Research Center through Grant NAG1-530. The authors are indebted to D. M. Bushnell and M. Y. Hussaini of NASA Langley Research Center for originally suggesting the problem and providing many stimulating discussions during the course of this study. The authors are thankful to C. M. Hung of NASA Ames Research Center for providing his three-dimensional Navier-Stokes code.

References

[1]Sedney, R., "A Survey of the Effects of Small Protuberances on Boundary Layer Flows," *AIAA Journal*, Vol. 11, No. 6, 1973, pp. 782–792.

[2]Sedney, R., and Kitchens, C. W., Jr., "Separation Ahead of Protuberances in Supersonic Turbulent Boundary Layers," *AIAA Journal*, Vol. 15, No. 4, 1977, pp. 546–552.

[3]Voitenko, D. M., Zubkov, A. I., and Panov, Y. A., "Supersonic Gas Flow Past a Cylindrical Obstacle on a Plate," *Mehanika ZhidkostiiGaza*, Vol. 1, Jan./Feb. 1966, pp. 121–125.

[4]Price, A. E., and Stallings, R. L., "Investigation of Turbulent Separated Flows in the Vicinity of Fin Type Protuberances at Supersonic Mach Numbers," NASA TN D-3804, Feb. 1967.

[5]Voitenko, D. M., Zubkov, A. I., and Panov, Y. A., "Influence of Mach Number on Flow in a Three-Dimensional Separation Region," *Moscow University Bulletin, Ser. I, Mathematics and Mechanics*, Vol. 23, No. 2, 1968, pp. 115–118.

[6]Uselton, J. C., "Fin Shock-Boundary Layer Interaction Tests on a Flat Plate with Blunted Fins at $M = 3$ and 5," Arnold Engineering Development Center TR-67-113, Arnold Air Force Station, Tullahoma, TN, June 1967.

[7]Westkaemper, J. C., "Turbulent Boundary Layer Separation Ahead of Cylinders," *AIAA Journal*, Vol. 6, No. 7, 1968, pp. 1352–1355.

[8]Lucas, E. J., "Investigation of Blunt Fin-Induced Flow Separation Region on a Flat Plate at Mach Numbers 2.5 to 4.0," Arnold Engineering Development Center TR-70-265, Arnold Air Force Station, Tullahoma, TN, Jan. 1971.

[9]Kaufman, L. G., Korkegi, R. H., and Morton, L. C., "Shock Impingement Caused by Boundary Layer Separation Ahead of Blunt Fins," Aeronautical Research Lab. 72-0118, Dayton, OH, Aug. 1972.

[10]Dolling, D. S., Cosad, C. D., and Bogdonoff, S. M., "An Examination of Blunt Fin-Induced Flows," AIAA Paper 78-159, Jan. 1978.

[11]Dolling, D. S., Cosad, C. D., and Bogdonoff, S. M., "An Examination of Blunt Fin-Induced Shock Wave Turbulent Boundary Layer Interactions," AIAA Paper 79-0068, Jan. 1979.

[12]Winkelmann, A. E., "Experimental Investigations of a Fin Protuberance Partially Immersed in a Turbulent Boundary Layer at Mach 5," Naval Ordinance Lab. TR-72-33, Silver Spring, MD, 1972.

[13]Gillerlain, J. D., "Fin-Cone Interference Flowfield," AIAA Paper 79-0200, Jan. 1979.

[14]Özcan, O., and Holt, M., "Supersonic Separated Flow Past a Cylindrical Obstacle on a Flat Plate," *AIAA Journal*, Vol. 22, No. 5, 1984, pp. 611–617.

[15]Hung, C. M., and Kordulla, W., "A Time-Split Finite-Volume Algorithm for Three-Dimensional Flowfield Simulation," *AIAA Journal*, Vol. 22, No. 11, 1984, pp. 1564–1572.

[16]Hung, C. M., and Buning, P. G., "Simulation of Blunt-Fin-Induced Shock Wave and Turbulent Boundary-Layer Interaction," *Journal of Fluid Mechanics*, Vol. 154, May 1985, pp. 163–185.

[17]Hung, C. M., "Computation of Separation Ahead of Blunt Fin in Supersonic Turbulent Flow," NASA TM-89416, Dec. 1986.

[18]Baldwin, B. S., and Lomax, H., "Thin Layer Approximation and Algebraic Model for Separated Turbulent Flows," AIAA Paper 78-257, Jan. 1978.

[19]Hung, C. M., and Kurasaki, S. S., "Thin-Layer Approximation for Three-Dimensional Supersonic Corner Flows," *AIAA Journal*, Vol. 18, No. 12, 1980, pp. 1544–1546.

[20]MacCormack, R. W., "The Effect of Viscosity in Hypervelocity Impact Cratering," AIAA Paper 69-354, May 1969.

[21]Lakshmanan, B., Tiwari, S. N., and Hussaini, M. Y., "A Parametric Study of Three-Dimensional Separation at a Wing/Body Junction for Supersonic Free-Stream Conditions," AIAA Paper 89-2198, July 1989.

[22]Young, F. L., Kaufmann, L. G., and Korkegi, R. H., "Experimental Investigation of Interaction Between Blunt Fin Shock Waves and Adjacent Boundary-Layers at Mach Numbers 3 and 5," Aerospace Research Lab. 68-0214, Dayton, OH, Dec. 1968.

[23]Baker, C. J., "The Laminar Horseshoe Vortex," *Journal of Fluid Mechanics*, Vol. 95, Pt. 2, Nov. 1979, pp. 347–367.

[24]Visbal, M. R., "Structure of Laminar Juncture Flows," *AIAA Journal*, Vol. 29, No. 8, 1991, pp. 1273–1282.